Isostatic and dynamic support of high topography on a North Atlantic passive margin

Vivi K. Pedersen [a],[*], Ritske S. Huismans [a], Robert Moucha [b]

[a] *Department of Earth Science, University of Bergen, Allegaten 41, N-5007 Bergen, Norway*
[b] *Department of Earth Sciences, Syracuse University, Syracuse, NY 13210, United States*

ARTICLE INFO

ABSTRACT

Substantial controversy surrounds the origin of high topography along passive continental margins. Here we focus on the well-documented elevated passive margin in southwestern Scandinavia, and quantify the relative contributions of crustal isostasy and dynamic topography in controlling the present topography. We find that majority of the topography is compensated by the crustal structure, suggesting a topographic age that is in accord with the 400 Myr old Caledonian orogenesis. In addition, we propose that dynamic uplift of ∼300 m has rejuvenated existing topography locally in the coastal region over the last 10 Myr. Such uplift, combined with a general sea level fall, can help explain a variety of observations that have traditionally been interpreted in favor of a peneplain uplift model. We conclude that high topography along the Scandinavian margin cannot represent remnants of a peneplain uplifted within the last 20 Myr. The topography must have been high since the Caledonian orogeny.

© 2016 Elsevier B.V. All rights reserved.

1. Introduction

A surprisingly significant part of global high topography is associated with rifted passive continental margins such as along the North Atlantic margins in Scandinavia and Greenland, the south Atlantic Brazilian and African margins, the east Australian margin, the Red Sea, and western India. A number of mechanisms have been suggested for such high topography to exist far beyond the most recent period of active rifting, including flexural isostasy related to i) lithosphere necking (Braun and Beaumont, 1989), ii) mechanical unloading during extension (Weissel and Karner, 1989), and iii) differential denudation (Gilchrist and Summerfield, 1990). Other mechanisms include underplating and intrusions in the lower crust (McKenzie, 1984), anticlinal, lithospheric folds caused by compression (Japsen et al., 2012), and the notion that topography may have survived orogenic collapse and rifting to leave again remnants from earlier orogenesis (Nielsen et al., 2009). However, a comprehensive understanding of why these margins are elevated today and whether they share a common origin remains enigmatic. Herein we focus on the well-documented southwestern Scandinavian margin in the North Atlantic as an archetype of an elevated passive continental margin.

The topography in western Scandinavia shows distinct high-elevation low-relief regions that have traditionally been interpreted as remnants of a Mesozoic peneplain uplifted in the Cenozoic (Fig. 1, Hypothesis 1, time frame T2–T3; e.g. Lidmar-Bergström et al., 2000). This interpretation has been supported by offshore studies identifying increased sedimentation in the Cenozoic, overburial of coast-proximal tilted sedimentary strata, and an angular unconformity at the base of the Quaternary (e.g. Japsen, 1988; Riis, 1996; Stuevold and Eldholm, 1996). However, it has also been recently suggested that prolonged climate-dependent erosion and isostatic uplift of old remnant topography from the Caledonian orogeny that survived Mesozoic and early Cenozoic rifting may equally well explain these key observations (Fig. 1, Hypothesis 2, T1–T3; Goledowski et al., 2012; Nielsen et al., 2009; Steer et al., 2012).

These diametrically opposing end-member hypotheses imply distinctly different crustal structure and degree of crustal compensation of present-day topography (Fig. 1). Peneplain formation requires complete erosion of existing topography to the degree where any crustal root has been obliterated. The peneplain in Hypothesis 1 should therefore be associated with a non-buoyant crust (Fig. 1, T2). This should also be the case for an uplifted peneplain (Fig. 1, T3). For the inherited remnant topography in Hypothesis 2, a thickened buoyant crust is expected to compensate all present-day topography (Fig. 1, T2–T3). We emphasize in this context, that a thin crust may compensate positive topography, if low-density material acts as a crustal root (mass deficit). Conversely, a thick

T1, all hypotheses:
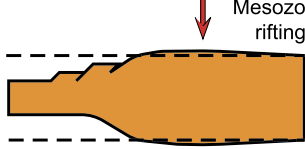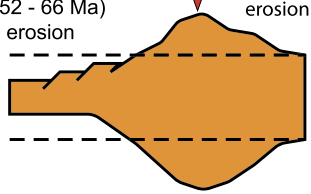Paleozoic Caledonian orogeny
490 - 390 Ma
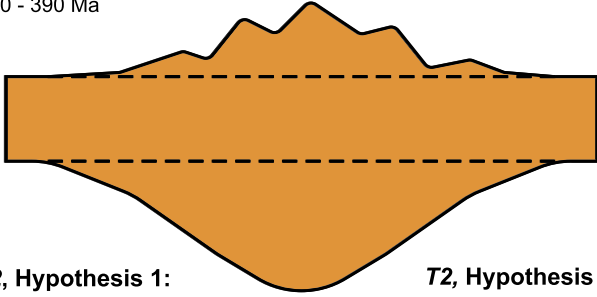
T2, Hypothesis 1:
Peneplanation

Mesozoic (252 - 66 Ma)
rifting and erosion

T2, Hypothesis 2:
Incomplete
erosion

T3, Hypothesis 1:
Uplift of peneplain
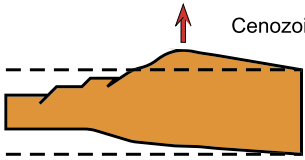
Cenozoic (66 - 0 Ma)

T3, Hypothesis 2:
erosion and isostatic uplift
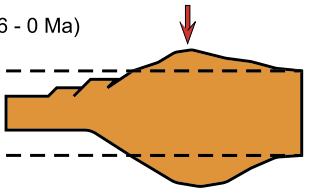
T3, Hypothesis 3 (this study):
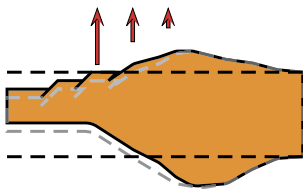Recent dynamic uplift (<10 Ma)
and incomplete erosion

Fig. 1. Schematic models for post-Caledonian geodynamic evolution in western Scandinavia. Existing hypotheses (Hypothesis 1 and Hypothesis 2) for the geodynamic evolution of western Scandinavia since the Caledonian orogeny illustrated by crust and topography structure at three snapshots in time (T1, T2, T3), and the hypothesis proposed in this study (Hypothesis 3). Dashed black lines represent a reference crustal thickness with zero compensated topography. Arrows indicate changes in surface elevation. Note figure is not to scale.

crust cannot necessarily compensate significant positive topography, if the buoyancy-effect of the crustal root is reduced by high-density material (mass excess).

The high topography along the Scandinavian margin roughly coincides with a significant negative (~ -85 mGal) Bouguer gravity anomaly (Fig. 2; Balling, 1980; Pavlis et al., 2012) and suggests that a mass deficit exists at depth. The relatively short wavelength of the gravity anomaly (~ 250 km) compared to crust- and lithosphere-thickness indicates that this mass deficit is located at shallow crustal depths and may compensate part or all of the present-day topography. However, the degree of compensation by the crustal structure is still debated, in part because an offset exists between the maximum topography and the thickest crust, and because of possible contributions from the lithospheric mantle and/or the asthenosphere (Ebbing and Olesen, 2005; Ebbing, 2007; Ebbing et al., 2012; England and Ebbing, 2012; Maupin et al., 2013; Stratford et al., 2009).

Here we quantify the degree of isostatic topographic compensation using refraction seismic data (Stratford et al., 2009) to constrain a hybrid approach considering crustal thickness (Airy isostasy), crustal density (Pratt isostasy), and the flexural strength of the lithosphere. We combine these quantitative estimates with predictions of recent dynamic uplift in order to test whether a combination of elements from previous end-member hypotheses may best explain the current high topography along this margin (Fig. 1, Hypothesis 3).

2. Methods

2.1. Local isostatic compensation of topography

We compute the degree of local isostatic compensation of present-day topography by the crustal structure with a three-dimensional density structure based on recently published seismic data from southern Norway (Stratford et al., 2009). These new seismic observations permit us to define a general velocity–depth relationship for this region by assuming a linear increase in velocity between four tie-points down through the crust (Fig. 3B). We convert this velocity model to density using a standard procedure described in Brocher (2005).

We calculate the amount of topography that can be compensated locally by the crust by balancing the load of each crustal column against a reference crustal column down to a common compensation depth where no lateral variation in density is assumed. That is,

$$\rho_{topo} h_{isostasy} g + \int_0^{moho} \rho_{crust}(z) g \, dz = \int_0^{Cref} \rho_{Cref}(z) g \, dz + \rho_m \Delta r g$$

where on the left-hand-side, the load of any local crustal column is given by the sum of the topographic load and the load of the crust. We assume a constant topographic load density ρ_{topo} of 2670 kg/m^3, corresponding to observed P-wave velocities at sea level. The crustal load is found by integrating the depth-dependent density profile $\rho_{crust}(z)$ from sea level down to the local *Moho* depth. On the right-hand-side, the reference column is defined as the load of a reference crust with thickness *Cref* and depth-dependent density profile, $\rho_{Cref}(z)$, plus a load from the mantle corresponding to any excess crust at the specific location ($\Delta r = moho - Cref$). The mantle lithosphere density ρ_m is assumed constant (3300 kg/m^3). With this load balance we can determine the local isostatically compensated topography $h_{isostasy}$:

$$h_{isostasy} = \frac{\int_0^{Cref} \rho_{Cref}(z)dz + \rho_m \Delta r - \int_0^{moho} \rho_{crust}(z)dz}{\rho_{topo}}.$$

For regions where the estimated isostatically compensated topography is less than zero, we substitute $h_{isostasy}$ with a corrected water depth d. The correction is done using the local depth-averaged crustal density, ρ_{avc}, iterating in order to consider the effect of the water depth, d, on the averaged crustal density itself, and the change in Moho thickness due to the water load.

$$d = \Delta a \frac{(\rho_m - \rho_{avc})}{(\rho_{avc} - \rho_w)}$$

where Δa is the thickness of the crustal deficit ($\Delta a = -\Delta r$) and ρ_w is the density of water.

The topography that can be locally compensated by a given crustal structure will depend on the choice of a reference crustal column that is assumed to give rise to zero topography. This is, however, inherently difficult to determine, because part of the topography may be due to buoyancy effects from within the mantle
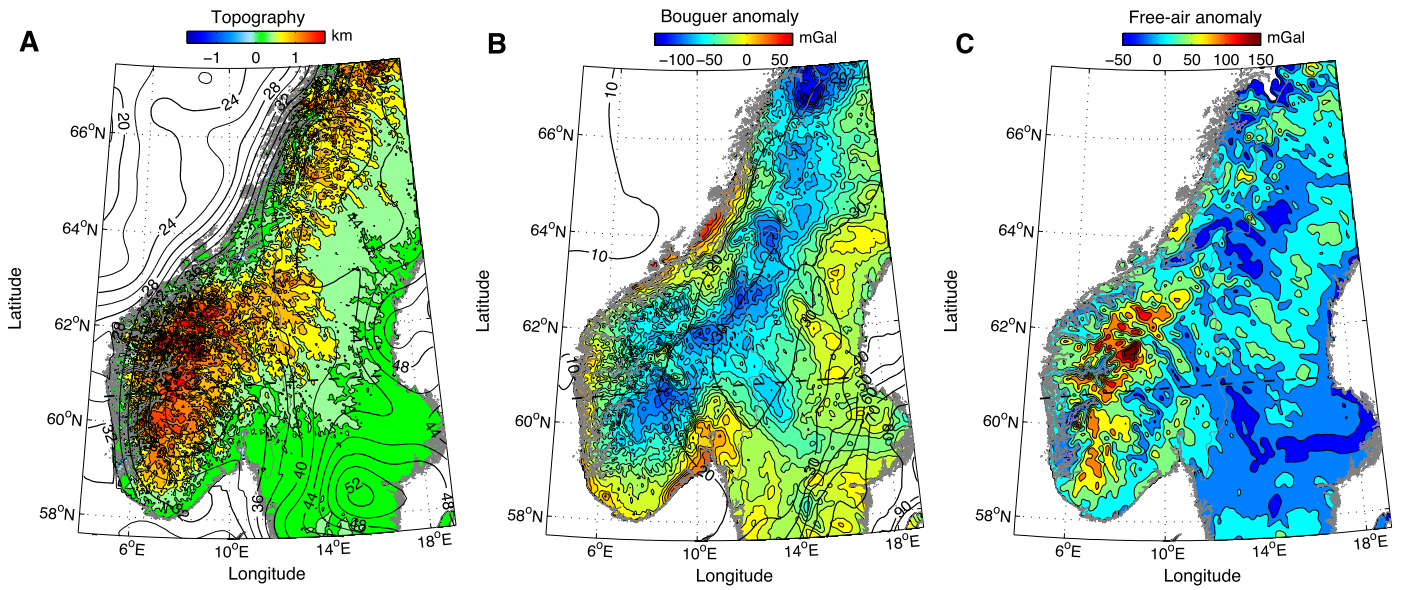
Fig. 2. Observations in Scandinavia. **A.** Colors indicate topography and bathymetry, whereas contour lines represent depth to the seismic Moho in km (Stratford et al., 2009). **B.** Colors represent Bouguer anomaly (http://bgi.omp.obs-mip.fr/; Fuella et al., 2008; Pavlis et al., 2012), whereas contours represent the effective elastic thickness in km (Pérez-Gussinyé and Watt, 2005). **C.** Colors represent free-air gravity anomaly (http://bgi.omp.obs-mip.fr/; Fuella et al., 2008; Pavlis et al., 2012).
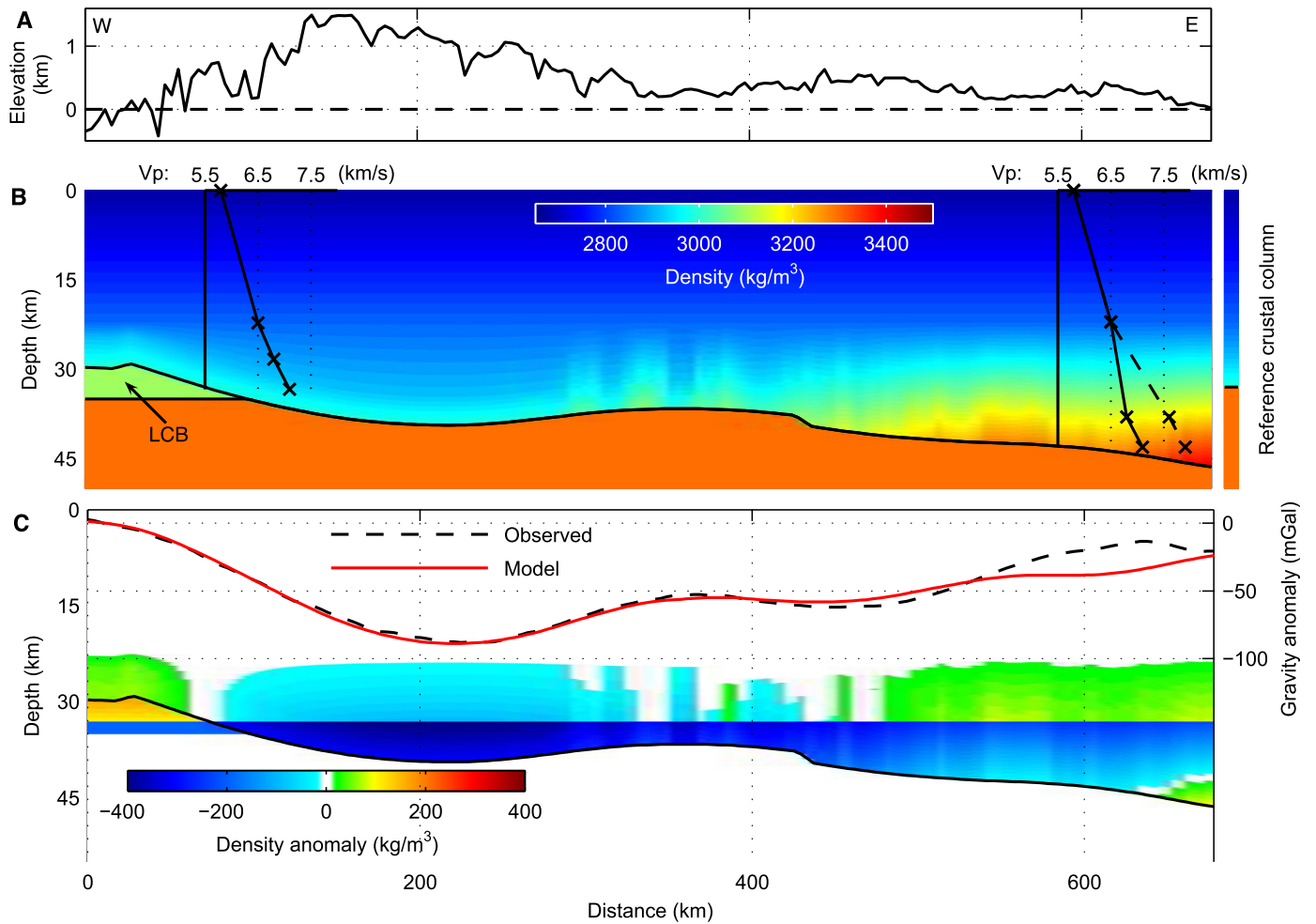
Fig. 3. Topography, density and gravity anomaly across southwestern Scandinavia. **A.** Elevation along transect (for location see Fig. 1). **B.** Density with depth along transect. Two vertical seismic velocity profiles illustrate the 4-point velocity model used to generate the density model. LCB indicates lower crustal body (see text). The reference crustal column is shown to the right. **C.** Density anomaly along transect with respect to reference crust (see **B**) and the resulting Bouguer gravity anomaly (red line) compared with the observed Bouguer gravity anomaly (black dashed line).

lithosphere and flexural effects that are not related to the local crust. We therefore constrain our reference crustal model by testing our approach for different reference Moho depths against the observed gravity anomaly below the high topography in southern Norway (Fig. 2B). The observed Gravity anomalies are available from BGI (http://bgi.omp.obs-mip.fr/); computed from the EGM2008 spherical harmonic coefficients (Pavlis et al., 2012) and topography- and Bouguer-corrected (Fuella et al., 2008). Model gravity anomalies are calculated using a spectral approach (Blakely, 1996). We find the best fit to the gravity anomaly with a reference Moho depth of ∼33 km (Fig. 3), whereas a reference Moho depth of either 30 km (Fig. S1A) or 35 km (Fig. S1B) leads to a predicted gravity anomaly below the high topography in southern Norway that is either too large or too small.

2.2. Correction of lower-crust velocities

Beyond southern Norway we increase lower-crustal velocities and corresponding densities when the estimated isostatically compensated topography is significantly higher than the observed topography (Fig. 3B, Fig. S2). Such a correction is required because our velocity model is constrained only by refraction seismic studies from southern Norway (Stratford et al., 2009). The correction is done by increasing the two lowermost tie-point velocities cell-wise in an iterative manner until predicted isostatic topography for the given cell or one of its neighboring cells is within a threshold of 50 m from the true topography (Fig. 3B). We find that this approach and choice of topographic threshold yields a good fit between observed and modeled gravity anomalies (Fig. 3C). This increase is also in accord with previous studies that proposed high-velocity, high-density lower crust in the thick, cold Baltic shield (Ebbing, 2007; Ebbing et al., 2012; England and Ebbing, 2012).

Moreover, offshore seismic observations and gravity modeling suggest that a high-velocity lower crustal body of partially eclogitized material is located at the coast of southern Norway (Christiansson et al., 2000). This implies that offshore and along the western coast of Norway, the seismically observed Moho does not correspond to the base of the crust, but rather to a change in velocity from 'normal' crust to a high-velocity lower crustal body. In order to match these seismic offshore observations and the gravity anomaly along the coastline (Fig. 3B–C), we include a high-density lower crustal body along the west coast of southern Norway from the seismically defined Moho down to a depth of 35 km (Fig. 3B, Fig. S3).

2.3. Regional isostatic compensation of topography

We also consider the effects of the lithosphere having a finite strength, by comparing the deflections that occur when loading a thin elastic plate with the positive load of the topography (mass excess) and the negative load of the crustal root (equivalent to a mass deficit at the surface), respectively (Fig. S5). We note that the topographic load will be negative in regions where fjord erosion has over-deepened the landscape. Because our crustal density model includes lateral variations we find this negative load of the mass deficit by first integrating the load of the entire crustal column and then subtracting the load of the corresponding reference column. In order to incorporate spatial variations in lithospheric strength (Fig. 1b), we adopt an Alternating-Direction-Implicit technique to solve for the flexural isostatic response of a given load (Pelletier, 2004). Model parameters used are Young's modulus (70 GPa) and Poisson's ratio (0.25). Herein we adopt the effective elastic thickness determined from Bouguer coherence analysis of northern Europe by Pérez-Gussinyé and Watt (2005).

The ratio between plate deflections resulting from the positive load of the topography and the negative load of the mass deficit at

depth (Supplementary Fig. S5) will give a measure of the degree of regional compensation, $pct_{compensated}$:

$$pct_{compensated} = \left(\frac{w_{root}}{w_{topo}} \right) \cdot 100\%$$

where w_{topo} is the deflection due to topography and w_{root} is the deflection due to the mass deficit at depth acting as a crustal root.

Non-compensated topography, on the other hand, is given by $pct_{non-compensated}$ (Fig. 3B):

$$pct_{non-compensated} = \left(1 - \frac{w_{root}}{w_{topo}} \right) \cdot 100\%$$

To calculate the regionally compensated topography (Fig. 3A), $pct_{compensated}$ is multiplied by the observed topography for onshore regions whereas in fjord regions it is found by interpolation from onshore regions. The non-compensated (i.e. residual) topography is then found as the difference between compensated topography and the observed topography (Fig. 3C). In regions where negative topography is predicted, we account for water loading as described above in 2.1.

2.4. Uncertainties in isostatic compensation of topography

Our calculations of isostatic compensation are based on estimates of crustal thickness that include inherent uncertainties (Stratford et al., 2009) as well as assumptions on: (i) reference crust, (ii) the extent and density of the high-velocity lower crustal body at the coastline (Christiansson et al., 2000), and (iii) the velocity structure beyond southern Norway where constraints from seismic refractions are limited (Stratford et al., 2009). Moreover, we have omitted possible contributions to isostasy from lateral density heterogeneity within the lithospheric mantle (Gradmann et al., 2013). Although constrained by observations of gravity, our three-dimensional density model is therefore inherently non-unique, especially due to the intrinsic trade-off between crustal density and thickness, and difficulties distinguishing buoyancy sources from the crust with those arising from the lithospheric mantle. We stress in this context that the relatively short wavelength of the gravity anomaly located under the high topography in southern Norway points to a buoyancy source in the crust.

Importantly, any combination of subsurface density structure and Moho thickness that satisfy the observed gravity anomaly should produce a similar degree of topographic compensation. As a consequence, the degree of isostatic compensation of topography we infer in this study should not change significantly as a result of additional future constraints on the subsurface density structure or by attributing part of the gravity signal from local buoyancy features in the lithospheric mantle.

2.5. Dynamic topography

Dynamic topography is defined as topography supported by vertical stresses due to viscous flow in the mantle (e.g. Braun, 2010). Herein, mantle flow and resulting dynamic topography is driven by density perturbations in the mantle, derived from joint inversions of global seismic and geodynamic data sets, including mineral physical constraints on the conversion of seismic velocities to densities (Simmons et al., 2007, 2009). A radially symmetric viscosity, inferred from joint inversions of global convection-related observables and glacial isostatic adjustment data, governs mantle flow (Mitrovica and Forte, 2004).

In order to include a measure of uncertainty related to this modeling, we include results from four different models, exploring two different density perturbation models (TX2007 vs. TX2008; Simmons et al., 2007, 2009) and two different depth-dependent

effective viscosity profiles (V1 vs. V2; Forte et al., 2010). Both density models fit global seismic and geodynamic data sets equally well and differences between the two models arise only from the inversion parameters used (Simmons et al., 2007, 2009). The two viscosity profiles also fit observations equally (Forte et al., 2010), with the greatest difference between V1 and V2 being a low viscosity notch in V1 between the upper and lower mantle (Forte et al., 2010). Results shown in the main text (Fig. 4D, 5) are based on the V1 viscosity model (Forte et al., 2010) and the TX2007 density model (Simmons et al., 2007). Additional models are evaluated in Supplementary Figs. S6–S8.

Predictions of absolute dynamic topography are highly influenced by the lithospheric mantle, which is often poorly constrained in terms of age, depletion/composition, and/or temperature. The convective models used in this study do include mineral physical constraints, and compositional effects are taken into account to some degree (Simmons et al., 2007, 2009). However, the use of a global seismic framework in the inversions is a limiting factor to the extent in which one may resolve regional lithospheric mantle heterogeneity. Therefore, we cannot expect the models to capture regional mantle lithosphere structures specific to the Scandinavian region (e.g. Gradmann et al., 2013; Maupin, 2011; Medhus et al., 2012; Rickers et al., 2013). We can ascertain that there is consensus between global and regional models at depth (below the lithosphere), however, for the lithospheric mantle this is not the case. For this reason, we remove contributions to dynamic topography from the upper 200 km, by assuming it neutrally buoyant (Fig. S6A–D). By doing so, we eliminate any contributions from the poorly constrained (global) lithospheric mantle to dynamic topography, and as a result get much more consistent predictions from the different model runs (Fig. S6E–H).

Regional studies suggest, however, that the uppermost mantle in the Scandinavian region may be positively buoyant (Gradmann et al., 2013; Maupin, 2011; Medhus et al., 2012; Rickers et al., 2013) compared to the reference density model used in the convection models (PREM; Dziewonski and Anderson, 1981). Such buoyancy, not captured by our global modeling approach, should result in negative dynamic topography predictions in southwestern Scandinavian when assuming the upper 200 km neutrally buoyant (Fig. S6). As an example, a density anomaly of $\sim$15 kg/m^3 will result in $\sim$500 m of topography if distributed within the upper 100 km, whereas a density anomaly of $<$10 kg/m^3 will result in $\sim$500 m of topography if distributed within the upper 200 km. These values are well within realistic density variations found in sub-continental lithospheric mantle (Djomani et al., 2001), and are consistent with expected values found for the Phanerozoic and Proterozoic mantle lithosphere below the Scandinavian region (Gradmann et al., 2013), compared to the reference density model (PREM; Dziewonski and Anderson, 1981).

The regional studies suggest also that there is a significant difference in the mantle lithosphere found below Norway and Sweden, respectively, owing to local variations in age, depletion, thickness, and temperature (Gradmann et al., 2013; Maupin, 2011; Medhus et al., 2012; Rickers et al., 2013). The mantle lithosphere below Sweden has been found to be thicker and colder than below Norway, but is also more depleted. A number of seismic tomography studies also predict low velocities immediately below the lithosphere in southern Norway, suggesting the presence of hot asthenosphere in this region (Maupin, 2011; Legendre et al., 2012; Medhus et al., 2012; Rickers et al., 2013). These lateral variations in temperature and composition may result in variable buoyancy from within the upper 200 km across the southwestern Scandinavian region, making absolute values of dynamic topography difficult to interpret even when removing contributions from the upper 200 km.

We therefore evaluate in the following only changes in dynamic topography over time (latest 10 Myr) using a backward-in-time convection scheme and taking into account tectonic plate motion (Moucha et al., 2008; Moucha and Forte, 2011). By considering changes in dynamic topography over time, we avoid uncertainties related to the lithospheric mantle, both in terms of constraining absolute buoyancy contribution, and in terms of understanding spatial variability within the region.

3. Results and discussion

In agreement with previous studies (Ebbing and Olesen, 2005; Ebbing, 2007; Ebbing et al., 2012; Maupin et al., 2013; Stratford et al., 2009; Stratford and Thybo, 2011), our isostatic calculations demonstrate that much of the current high topography in western Scandinavia can be explained by the crustal structure (Fig. 4A). This suggests that significant, more than 1000 m high topography has existed in the region since the formation of the current crustal structure. In contrast, the western-most part of southern Norway shows negative predictions of isostatically compensated topography (Fig. 4A) and indicates that the current topography in this area is poorly explained by crustal structure. Consequently, the residual topography ranges locally from fully compensated in the high-elevated areas in central southern Norway to completely uncompensated ($+1000$ m) along the west coast (Fig. 4C). Much of this local variability may be ascribed to lithology, rock strength, and differential erosion, and most regions show less extreme values, with a general trend of decreasing isostatic compensation toward the west coast (Fig. 4B). On average $\sim$300 m of topography is uncompensated by the current crustal structure in southwestern Norway.

Accordingly, a mechanism unrelated to crustal structure is needed in order to explain the uncompensated residual topography found in southwestern Norway ($\sim$300 m), and observed low velocities in the upper mantle may suggest a dynamic origin related to mantle flow (Maupin, 2011; Medhus et al., 2012; Rickers et al., 2013). A sub-lithospheric origin linked to convection could also explain the generally positive free-air gravity anomaly in this part of the region (Fig. 2C; Molnar et al., 2015).

Spatial patterns in dynamic topography change in Scandinavia over the last 10 Myr are remarkably consistent between the different evaluated models, showing positive values in southern Norway and close to zero or negative values in the rest of the region (Fig. 4D, Fig. S7). This is in agreement with previous work from the broader region (Steinberger et al., 2015; Marquart and Schmeling, 2004) and suggests dynamic surface uplift for southwestern Norway within the last 10 Myr, with an increasing trend toward the coast, and concurrent dynamic subsidence that increases toward the east (Fig. 4D, Fig. S7).

As illustrated by the variability in amplitudes between the models, absolute values of dynamic topography are difficult to assess, as minor uniform regional changes in density may shift absolute values without significantly degrading the global fit to the models' geodynamic constraints (Fig. S7; Forte et al., 2010). Long wavelength spatial gradients in dynamic topography are, however, more robust as they arise from the large-scale flow field that is consistent with the long wavelength geodynamic constraints. We find consistently for all evaluated models an uplift gradient of $\sim$200–300 m from east to west in southwestern Scandinavia (Fig. 4D, Fig. S7). These dynamic surface motions are predicted as a consequence of passive upwelling below the southern margin of Norway that is part of a larger convective cell as shown in the regional cross-sections (Fig. 5, Fig. S8).

The strong correlation in both spatial distribution and amplitude between isostatic residual topography (Fig. 4B–C) and recent changes in dynamic topography (Fig. 4D) suggests local rejuvena-
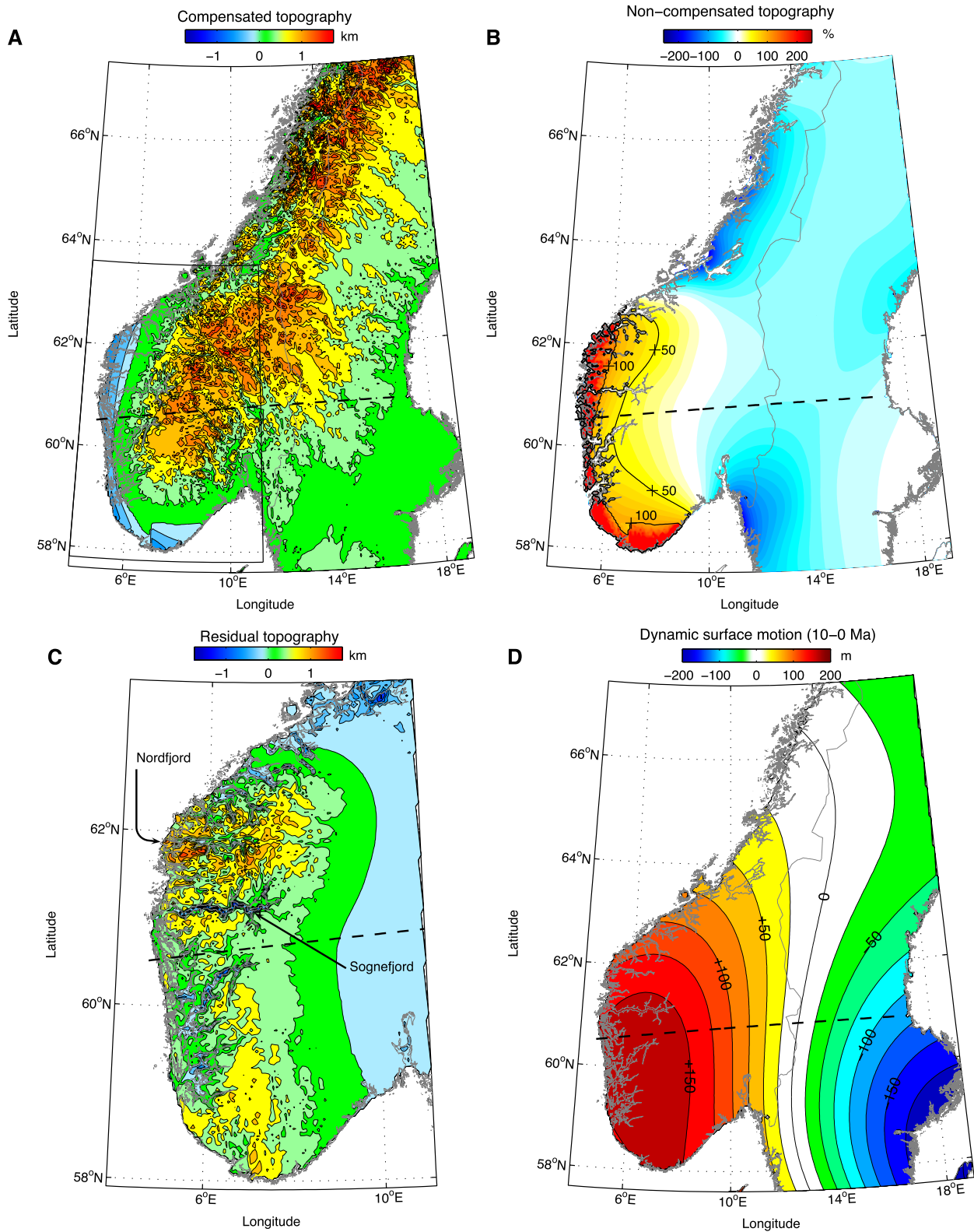
Fig. 4. Regional isostatic, residual, and dynamic topography. **A.** Topography compensated by the crust. Regions with negative predicted topography have been corrected for water load. **B.** Degree of topography not compensated by the crust. Contour lines represent 50% and 100% non-compensation. **C.** Residual topography (real topography minus isostatically compensated topography from **A**). Positive values represent regions where the present topography is higher than expected from the crustal structure, and negative values regions where the topography is lower than expected. **D.** Dynamic topography change since 10 Ma (TX2007V1; Simmons et al., 2007; Forte et al., 2010). Positive values indicate rock uplift whereas negative values correspond to subsidence. Black dashed line represents the profile shown in Fig. 2.
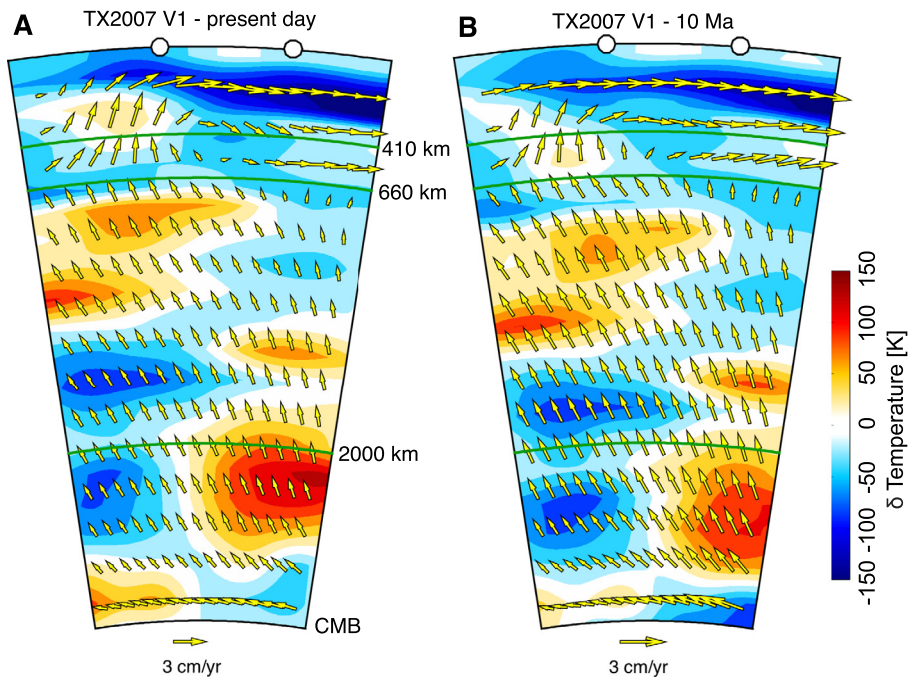
Fig. 5. Mantle temperature structure and flow. **A.** Present-day thermal structure derived from the TX2007 density model (Simmons et al., 2007), with mantle flow calculated for the V1 viscosity model (Forte et al., 2010). The cross-section coincides with the cross-section shown in Figs. 2–4 of the main text, with the points at the surface marking the west coast of Norway (4.6E, 60.5N) and east coast of Sweden (17.0E, 60.9N), respectively. **B.** Corresponding backwards advected mantle temperatures and mantle flow at 10 Ma. The green in lines across the sections are depth markers at: 410 km, 660 km, and 2000 km. The base of the figure represents the core–mantle boundary (CMB).

tion of already existing topography in southwestern Norway during the last 10 Myr. The uplift is mostly prevalent near the coastal regions and decreases inland toward the highest topography that appears to be largely compensated by the crustal structure.

In this study we have not considered explicitly buoyancy-contributions from the lithospheric mantle. However, lateral variations in density owing to a spatially varying lithospheric thickness may contribute to compensate the present topography. Indeed, following previous work by Gradmann et al. (2013), a lithospheric thinning of ∼30 km across southern Norway could account for some (∼100–200 m) of the inferred residual topography (Fig. 4C), if a density contrast of ∼10–20 kg/m^3 is assumed across the lithosphere–asthenosphere boundary (LAB), as suggested by geodynamic modeling in the region (Gradmann et al., 2013). Such minor long-wavelength features may not be captured in the gravity anomaly map and resolved by the gravity modeling approach used, and should therefore be considered in addition to the isostatic compensation found in this study. More significant buoyancy contributions from within the lithospheric mantle should be recognizable from the gravity anomaly, and such contributions are therefore already accounted for in our approach (see section 2.4).

Topography compensated by a density contrast across the LAB for a spatially varying lithosphere thickness could be related to the original lithospheric architecture in the region or to erosion at the base of the lithosphere by small-scale mantle convection. We note in this context that our inferred residual topography (Fig. 4C) shows an increasing trend toward the North Sea basin and not the current spreading axis in the north Atlantic. This may suggest that any base-lithosphere erosion was related to rifting in the North Sea in Mesozoic times (e.g. Glennie, 1998), as opposed to more recent Cenozoic events in the north Atlantic. Therefore, we do not rule out that buoyancy contributions from the lithospheric mantle may contribute to the present topography. However, we suspect that such contributions predate recent (<10 Ma) dynamic surface uplift inferred in this study.

Our results provide strong support for an old Caledonian age of most high topography in western Scandinavia, given that the most

recent crustal thickening occurred during the Caledonian orogeny. However, a component of the topography along the west coast of southern Norway is found not to be in isostatic equilibrium. Although of moderate amplitude (in average ∼300 m), this result is well constrained by the observed gravity anomaly in southwestern Scandinavia, and it is therefore a robust outcome, regardless of the uncertainly associated with the crustal model in use.

By suggesting significant isostatic support of the high mountains in southern Norway, in combination with recent modest dynamic topographic rejuvenation of the coastal area, our hypothesis includes components from both previous hypotheses for long-term topographic evolution in western Scandinavia (Fig. 1, Hypothesis 3). Although of amplitude much smaller than previously suggested by the peneplain hypothesis (Fig. 1, Hypothesis 1), recent dynamic uplift of the coastal areas in southern Norway provides an additional mechanism of uplift to the isostatic rock-column uplift expected as a consequence of erosional unloading. This modest topographic rejuvenation is, in combination with a general eustatic sea-level fall (Miller et al., 2005) and concurrent erosion-driven isostatic rock-column uplift, consistent with observations of increased sedimentation since ∼10 Ma, over-burial of coast-proximal tilted sedimentary strata, and an angular unconformity at the base of the Quaternary (e.g. Japsen, 1988; Riis, 1996; Stuevold and Eldholm, 1996). As previously suggested by Nielsen et al. (2009), these offshore observation may be explained by climate-dependent erosion-driven rock-column uplift in the onshore and offshore subsidence due to sediment loading, in combination with recent glacial reworking of shelf sediments. However, from the study presented here, we have good reason to believe that some part of the offshore signal is due to a modest dynamic uplift of the coastal region, and the exposure and reworking of shelf sediments that this would have facilitated.

Our results show that high-elevation low-relief regions in western Scandinavia cannot represent a dissected Mesozoic peneplain uplifted in Neogene times. Recent peneplain uplift is simply incompatible with the large degree of isostatic support of topography we find in this study. We suggest that low-relief regions in western

Scandinavia represent a generally low-relief landscape (a remnant of Caledonian topography) that has experienced glacial erosion at high elevation (Pedersen and Egholm, 2013; Steer et al., 2012) and been smoothened by altitudinal-dependent periglacial processes (Anderson, 2002; Egholm et al., 2015). The low relief landscape has been dissected by fluvial and glacial activity – processes that have been amplified by (i) a general eustatic sea level fall since the Cretaceous (Miller et al., 2005), (ii) modest dynamic uplift since the Neogene owing to mantle convection (∼300 m), and last but not least (iii) climate cooling leading to substantial isostatic uplift resulting from unloading by differential glacial erosion.

4. Conclusions

Globally, the origin of elevated rifted passive continental margins is enigmatic and highly debated with a range of competing hypotheses. By quantifying contributions from crustal isostasy and dynamic topography in southwestern Scandinavia we constrain age, origin, and recent evolution of topography in this region. By providing a quantitative explanation that combines elements from pre-existing end-member hypotheses, the results presented here provide a new perspective on the long-standing controversy on the origin of high passive-margin topography in Scandinavia. Remnant topography from the Caledonian orogeny, modified by North Atlantic rifting and influenced by recent dynamic surface motions, control present-day topography along this continental margin.

Based on our results we reject the century-old idea of an uplifted, dissected peneplain existing in western Scandinavia. Recent peneplain uplift is simply incompatible with the large degree of isostatic support of topography we find in this study.

Acknowledgements

Appendix A. Supplementary material

Supplementary material related to this article can be found online at http://dx.doi.org/10.1016/j.epsl.2016.04.019.

References

Anderson, R.S., 2002. Modeling the tor-dotted crests, bedrock edges, and parabolic profiles of high alpine surfaces of the Wind River Range, Wyoming. Geomorphology 46, 35–58.

Balling, N., 1980. The land uplift in Fennoscandia, gravity field anomalies and isostasy. In: Mörner, N.-A. (Ed.), Earth Rheology, Isostasy and Eustasy. Wiley, New York, pp. 297–321.

Blakely, R.J., 1996. Fourier-domain modeling. In: Potential Theory in Gravity and Magnetic Applications. Cambridge Univ. Press, Cambridge, UK, pp. 258–310.

Braun, J., 2010. The many surface expressions of mantle dynamics. Nat. Geosci. 3, 825–833.

Braun, J., Beaumont, C., 1989. A physical explanation of the relation between flank uplifts and the breakup unconformity at rifted continental margins. Geology 17, 760–764.

Brocher, T.M., 2005. Empirical relations between elastic wavespeeds and density in the Earth's crust. Bull. Seismol. Soc. Am. 96 (6), 2081–2092.

Christiansson, P., Faleide, J.I., Berge, A.M., 2000. Crustal structure in the northern North Sea: an integrated geophysical study. In: Nøttvedt, A. (Ed.), Dynamics of the Norwegian Margin. In: Geol. Soc. (Lond.) Spec. Publ., vol. 167. Geological Society, London, pp. 15–40.

Djomani, Y.H.P., O'Reilly, S.Y., Griffin, W.L., Morgan, P., 2001. The density structure of subcontinental lithosphere through time. Earth Planet. Sci. Lett. 184, 605–621.

Dziewonski, A.M., Anderson, D.L., 1981. Preliminary reference Earth model. Phys. Earth Planet. Inter. 25, 297–356.

Ebbing, J., Olesen, O., 2005. The Northern and Southern Scandes – structural differences revealed by an analysis of gravity anomalies, the geoid and regional isostasy. Tectonophysics 411, 73–87.

Ebbing, J., 2007. Isostatic density modeling explains the missing root of the Scandes. Norwegian J. Geol. 87, 13–20.

Ebbing, J., et al., 2012. Structure of the Scandes lithosphere from surface to depth. Tectonophysics 536–537, 1–24.

Egholm, D.L., Andersen, J.L., Knudsen, M.F., Jansen, J.D., Nielsen, S.B., 2015. The periglacial engine of mountain erosion – Part 2: modelling large-scale landscape evolution. Earth Surf. Dynam. 3, 463–482.

England, R.W., Ebbing, J., 2012. Crustal structure of central Norway and Sweden from integrated modeling of teleseismic receiver functions and the gravity anomaly. Geophys. J. Int. 191, 1–11.

Forte, A.M., et al., 2010. Joint seismic–geodynamic-mineral physical modelling of African geodynamics: a reconciliation of deep-mantle convection with surface geophysical constraints. Earth Planet. Sci. Lett. 295, 329–341.

Fuella, J., Fernandez, M., Zeyen, H., 2008. FA2BOUG – a FORTRAN 90 code to compute Bouguer gravity anomalies from gridded free-air anomalies: application to the Atlantic–Mediterranean transition zone. Comput. Geosci. 34 (12), 1665–1681.

Gilchrist, A.R., Summerfield, M.A., 1990. Differential denudation and flexural isostasy in formation of rifted-margin upwarps. Nature 346, 739–742.

Glennie, K.W., 1998. Petroleum Geology of the North Sea: Basic Concepts and Recent Advances, 4th ed. Blackwell Science Ltd.

Goledowski, B., Nielsen, S.B., Clausen, O.R., 2012. Patterns of Cenozoic sediment flux from western Scandinavia. Basin Res. 24, 377–400.

Gradmann, S., Ebbing, J., Fuella, J., 2013. Integrated geophysical modeling of a lateral transition zone in the lithospheric mantle under Norway and Sweden. Geophys. J. Int. 194, 1358–1378.

Japsen, P., 1988. Regional velocity-depth anomalies, North Sea Chalk: a record of overpressure and Neogene uplift and erosion. Am. Assoc. Pet. Geol. Bull. 82 (11), 2031–2074.

Japsen, P., Chalmers, J.A., Green, P.F., Bonow, J.M., 2012. Elevated, passive continental margins: not rift shoulders, but expressions of episodic, post-rift burial and exhumation. Glob. Planet. Change 90–91, 73–86.

Legendre, C.P., et al., 2012. A shear wave velocity model of the European upper mantle from automated inversion of seismic shear and surface waveforms. Geophys. J. Int. 191, 282–304.

Lidmar-Bergström, K., Ollier, C.D., Sulebak, J.R., 2000. Landforms and uplift history of southern Norway. Glob. Planet. Change 24, 211–231.

Marquart, G., Schmeling, H., 2004. A dynamic model for the Iceland Plume and the North Atlantic based on topography and gravity data. Geophys. J. Int. 159, 40–52.

Maupin, V., 2011. Upper-mantle structure in southen Norway from beamforming of Rayleigh wave data presenting multipathing. Geophys. J. Int. 185, 985–1002.

Maupin, V., et al., 2013. The deep structure of the Scandes and its relation to tectonic history and present-day topography. Tectonophysics 602, 15–37.

McKenzie, D., 1984. A possible mechanism for epeirogenic uplift. Nature 307, 616–618.

Medhus, A.B., et al., 2012. Upper-mantle structure beneath the Southern Scandes Mountains and the Northern Tornquist Zone revealed by P-wave traveltime tomography. Geophys. J. Int. 189, 1315–1334.

Miller, K.G., et al., 2005. The phanerozoic record of global sea-level change. Science 310, 1293–1298.

Mitrovica, J.X., Forte, A.M., 2004. A new inference of mantle viscosity based upon joint inversion of convection and glacial isostatic adjustment data. Earth Planet. Sci. Lett. 225 (1–2), 177–189.

Molnar, P., England, P.C., Jones, C.H., 2015. Mantle dynamics, isostasy, and the support of high terrain. J. Geophys. Res., Solid Earth 120, 1932–1957.

Moucha, R., et al., 2008. Mantle convection and the recent evolution of the Colorado Plateau and the Rio Grande Rift valley. Geology 36 (6), 439–442.

Moucha, R., Forte, A.M., 2011. Changes in African topography driven by mantle convection. Nat. Geosci. 4, 707–711.

Nielsen, S.B., et al., 2009. The evolution of western Scandinavian topography: a review of Neogene uplift versus the ICE (isostasy–climate–erosion) hypothesis. J. Geodyn. 47 (2–3), 72–95.

Pavlis, N.K., Holmes, S.A., Kenyon, S.C., Factor, J.K., 2012. The development and evaluation of the Earth Gravitational Model 2008 (EGM2008). J. Geophys. Res. 117 (B04406).

Pedersen, V.K., Egholm, D.L., 2013. Glaciations in response to climate variations preconditioned by evolving topography. Nature 493, 206–210.

Pelletier, J.D., 2004. Estimates of three-dimensional flexure-isostatic response to unloading: rock uplift due to late Cenozoic glacial erosion in the western United States. Geology 32, 161–164.

Pérez-Gussinyé, M., Watt, A.B., 2005. The long-term strength of Europe and its implications for plate-forming processes. Nature 436, 381–384.

Rickers, F., Fichtner, A., Trampert, J., 2013. The Iceland—Jan Mayen plume system and its impact on mantle dynamics in the North Atlantic region: evidence from full-waveform inversion. Earth Planet. Sci. Lett. 367, 39–51.

Riis, F., 1996. Quantification of Cenozoic vertical movements of Scandinavia by correlation of morphological surfaces with offshore data. Glob. Planet. Change 12, 331–357.

Simmons, N.A., Forte, A.M., Grand, S.P., 2007. Thermochemical structure and dynamics of the African super-plume. Geophys. Res. Lett. 34, L02301.

Simmons, N.A., Forte, A.M., Grand, S.P., 2009. Joint seismic, geodynamic and mineral physical constraints on three-dimensional mantle heterogeneity: implications for the relative importance of thermal versus compositional heterogeneity. Geophys. J. Int. 17, 1284–1304.

Steer, P., Huismans, R.S., Valla, P.G., Gac, S., Herman, F., 2012. Bimodal Plio-Quaternary glacial erosion of fjords and low-relief surfaces in Scandinavia. Nat. Geosci. 5, 635–639.

Steinberger, B., Spakman, W., Japsen, P., Torsvik, T.H., 2015. The key role of global solid-Earth processes in preconditioning Greenland's glaciation since the Pliocene. Terra Nova 27, 1–8.

Stratford, W., Thybo, H., Faleide, J.I., Olesen, O., Tryggvason, A., 2009. New Moho Map for onshore southern Norway. Geophys. J. Int. 178, 1755–1765.

Stratford, W., Thybo, H., 2011. Seismic structure and composition of the crust beneath the southern Scandes, Norway. Tectonophysics 502, 364–382.

Stuevold, L.M., Eldholm, O., 1996. Cenozoic uplift of Fennoscandia inferred from a study of the mid-Norwegian margin. Glob. Planet. Change 12, 359–386.

Weissel, J.K., Karner, G.D., 1989. Uplift of rift flanks due to mechanical unloading of the lithosphere during extension. J. Geophys. Res. 94 (B10), 13919–13950.